Qualification of operating conditions to extend oxygen carrier utilization in the scaling up of chemical looping processes

Arturo Cabello, Alberto Abad*, María T. Izquierdo, P. Gayán, Luis F. de Diego, Francisco García-Labiano, Juan Adánez

Instituto de Carboquímica (ICB-CSIC), Miguel Luesma Castán 4, 50018 Zaragoza, Spain

* Corresponding author:

e-mail address: abad@icb.csic.es (A. Abad); Phone: +34 976 733977; Fax: +34 976 733318

Supplementary material

Index

S.1. Operating conditions and results achieved with the Cu14Al_ICB and Cu14Al_Commercial oxygen carriers in continuous CLC units

Table S1. Summary of operational experience in CLC units with copper-based oxygen carriers burning gaseous fuels.

Oxygen carrier	CLC unit	Temperature FR-AR (°C)	ϕ interval	ΔX_s	Combustion time (h)	Number of redox cycles	Estimated lifetime (h)	Ref.
Cu14Al_ICB	10 kW ICB-CSIC	800-800	0.7-2.1	0.5-1.0	60	450	2400	[1-3]
	0.5 kW ICB-CSIC	800-800	5-10	0.1-0.2	63	630	n.a.	[4]
	0.5 kW ICB-CSIC	800-850	1.3-2.5	0.4-0.8	40	180	n.a.	[5]
	0.5 kW ICB-CSIC	800-900	1.0-1.2	0.7-0.8	63	273	1100	[6]
	0.5 kW ICB-CSIC	800-900	1.3-1.9	0.5-0.8	20	150	n.a.	[7]
	0.5 kW ICB-CSIC	800-950	1.0-2.4	0.4-0.9	39	200	5000	[8]
	0.5 kW ICB-CSIC	800-950	1.0-1.6	0.6-0.8	42	182	<200	[6]
	0.5 kW ICB-CSIC	800-950	1.0-1.5	0.65	15	80	n.a.	[9]
	120 kW TUWien	850-850	0.8-2.2	0.3-0.9	70	1200	n.a.	[10]
	50 kW TUHH	850-850	0.5-5.0	0.2-0.7	1	n.a.	770	[11]
	0.5 kW ICB-CSIC	900-900	1.0-1.2	0.8-0.97	48	208	<400	[6]
	0.5 kW ICB-CSIC	900-900	5-10	0.1-0.2	65	650	n.a.	[4]
	0.5 kW ICB-CSIC	880-950	1.0-1.3	0.8-0.9	15	100	n.a.	[9]
	0.5 kW ICB-CSIC	900-950	1.0-1.4	0.7-0.97	29	126	<150	[6]
TOTAL					570			
Cu14Al_Commercial	0.5 kW ICB-CSIC	800-800	1.2-2.6	0.4-0.8	60	700	5000	[12]
	120 kW TUWien	800-800	1.0-2.0	0.4-0.7	50	n.a.	n.a.	[13]
	150 kW SINTEF	850-850	0.8-5.0	0.2-0.7	5	184	n.a.	[14]
	0.5 kW ICB-CSIC	900-900	1.0-2.0	0.5-0.98	65	596	Low	[12]
	10 kW IFPEN	900-900	0.8-1.2	0.7-0.95	160	276	7200	[15]
TOTAL					340			

ICB-CSIC: Instituto de Carboquimica (CSIC, Spain)
IFPEN: IFP Energies nouvelles (France)
SINTEF: Stiftelsen for Industriell og Teknisk Forskning (Norway)
TUHH: Technische Universität Hamburg (Germany)
TUWien: Technische Universität Wien (Austria)

S.2. Redox cycles with the highly oxidized oxygen carrier at 800 °C

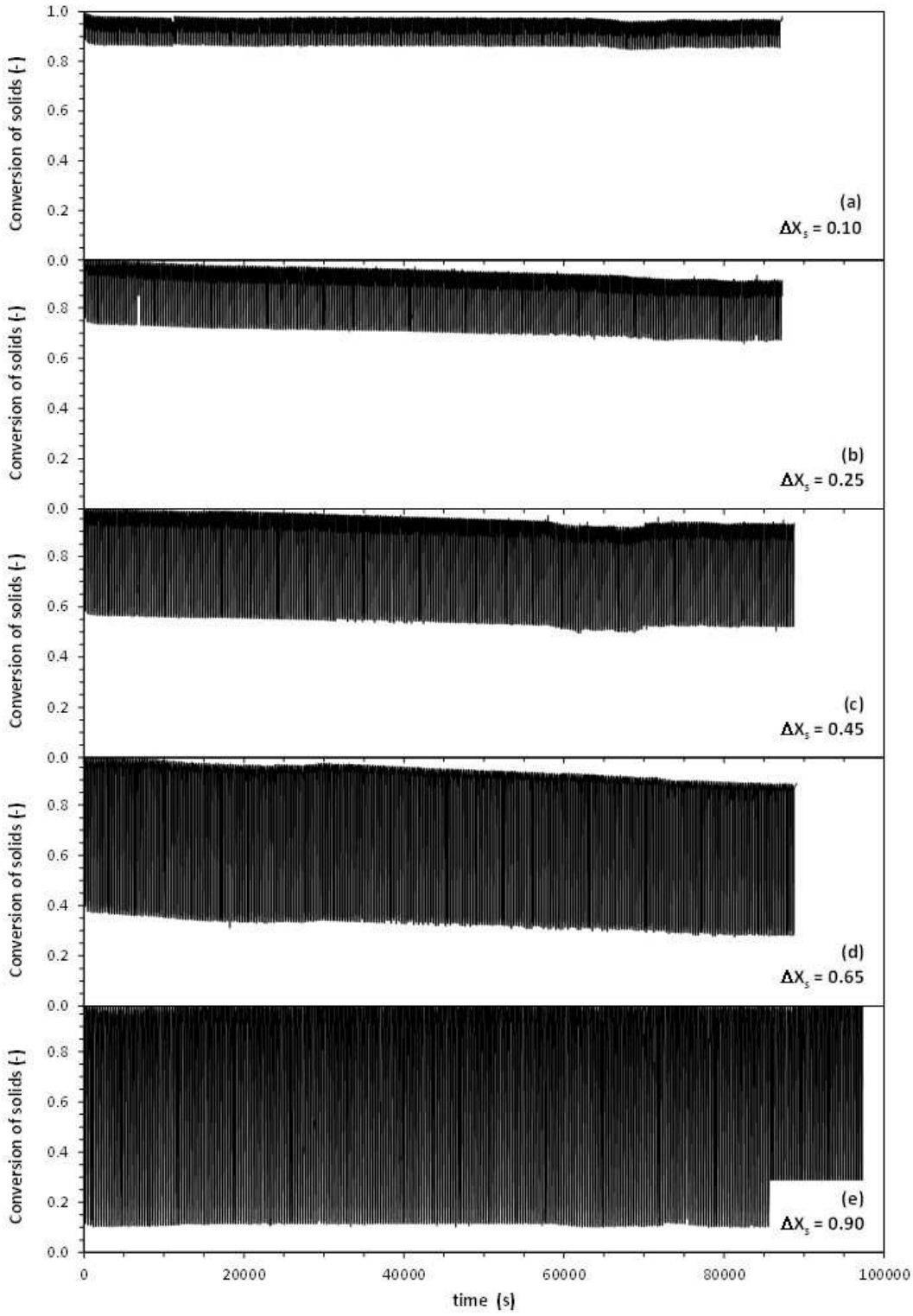

Figure S1. Evolution of solids conversion (defined for the oxidation state) during the redox cycles performed at different ΔX_s values with the oxygen carrier highly oxidized after each redox cycle. Reaction temperature: 800 °C.

S.3. Redox cycles with the highly oxidized oxygen carrier at 900 °C

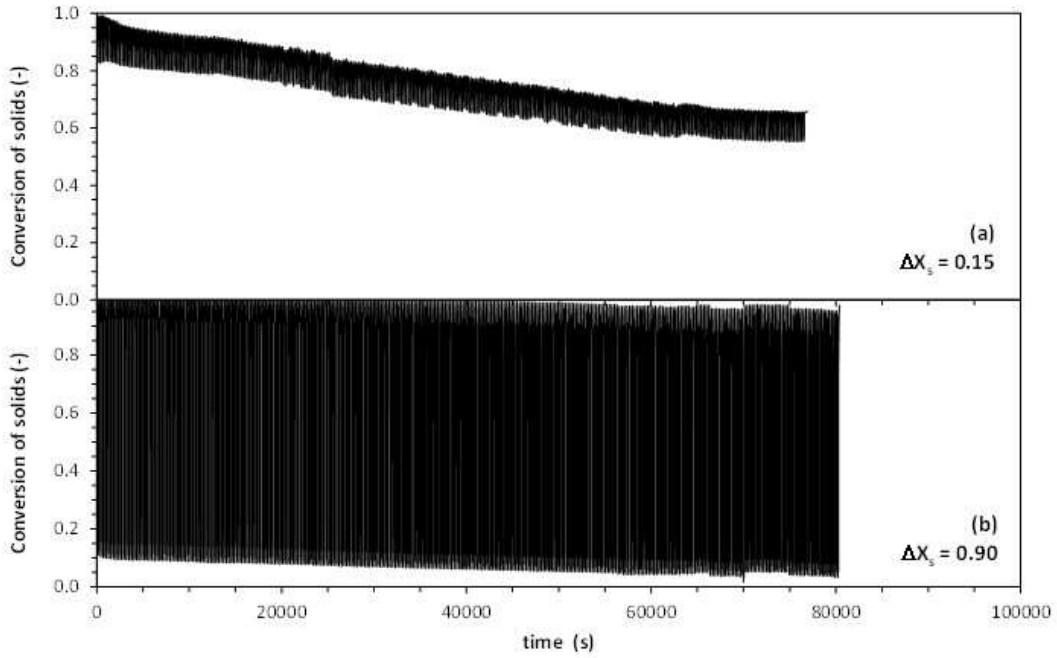

Figure S2. Evolution of the solids conversion (defined for the oxidation state) during the redox cycles performed at different ΔX_s values with the oxygen carrier highly oxidized after each redox cycle. Reaction temperature: 900 °C.

S.4. XRD patterns corresponding to the highly oxidized oxygen carrier at 800 °C

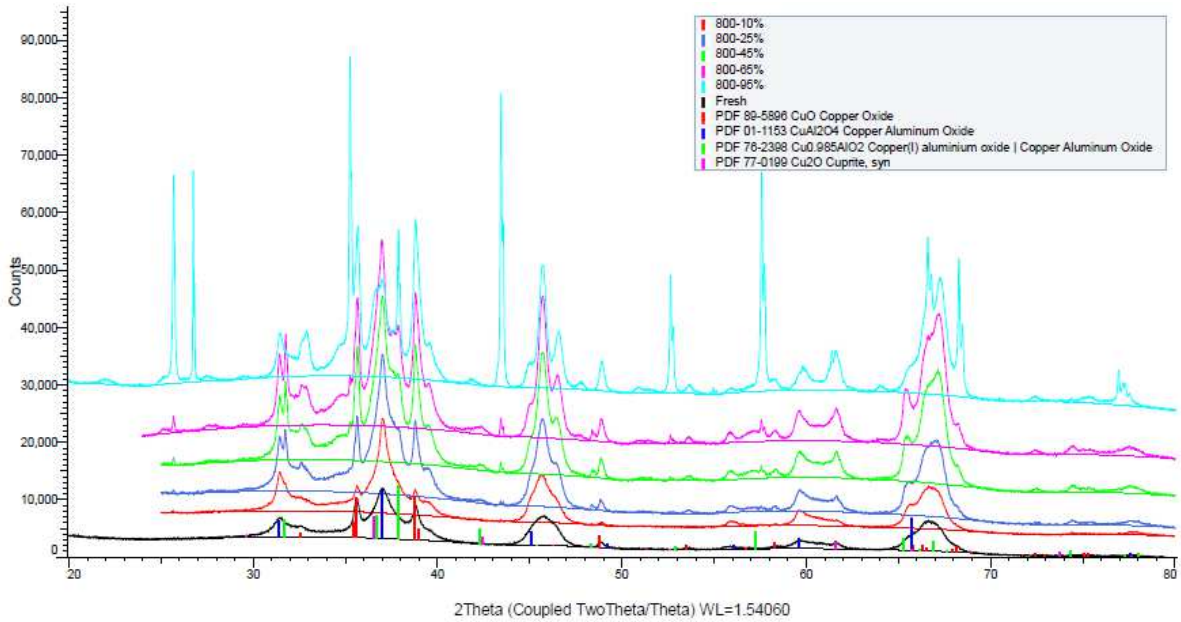

Figure S3. XRD diffractograms of the samples corresponding to the TGA tests performed at 800 ºC with the highly oxidized Cu14Al_ICB oxygen carrier (only Cu-compounds are tagged).

S.5. XRD patterns corresponding to the highly oxidized oxygen carrier at 900 °C

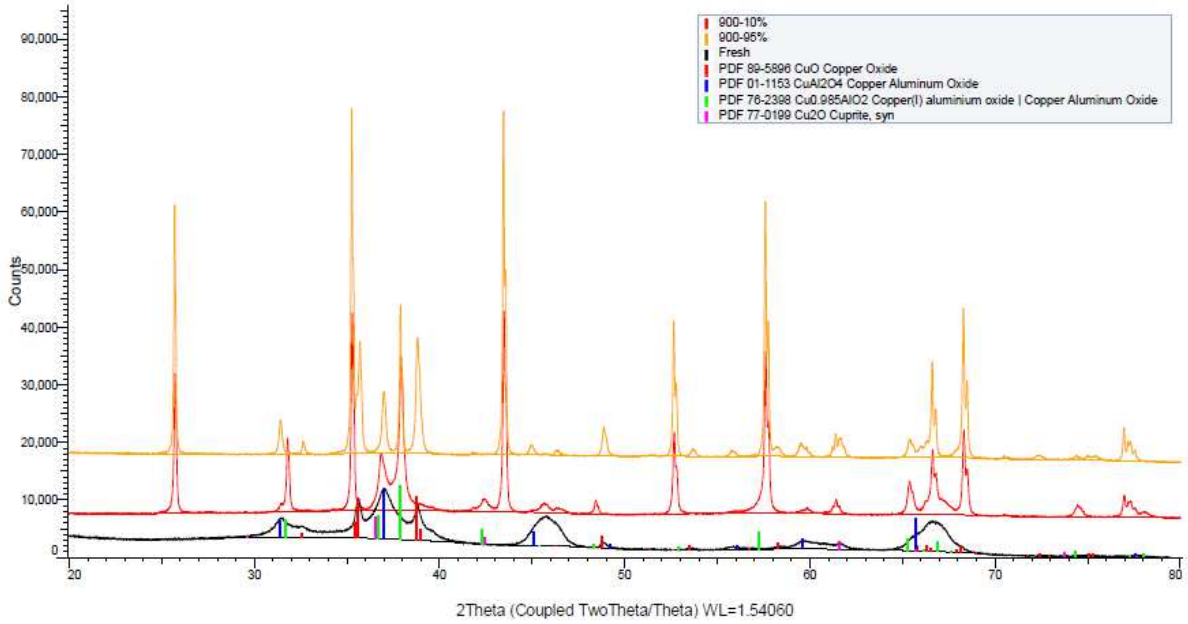

Figure S4. XRD diffractograms of the samples corresponding to the TGA tests performed at 900 ºC with the highly oxidized Cu14Al_ICB oxygen carrier (only Cu-compounds are tagged).

S.6. SEM images of used particles after redox cycles with the highly oxidized oxygen carrier at 800 °C

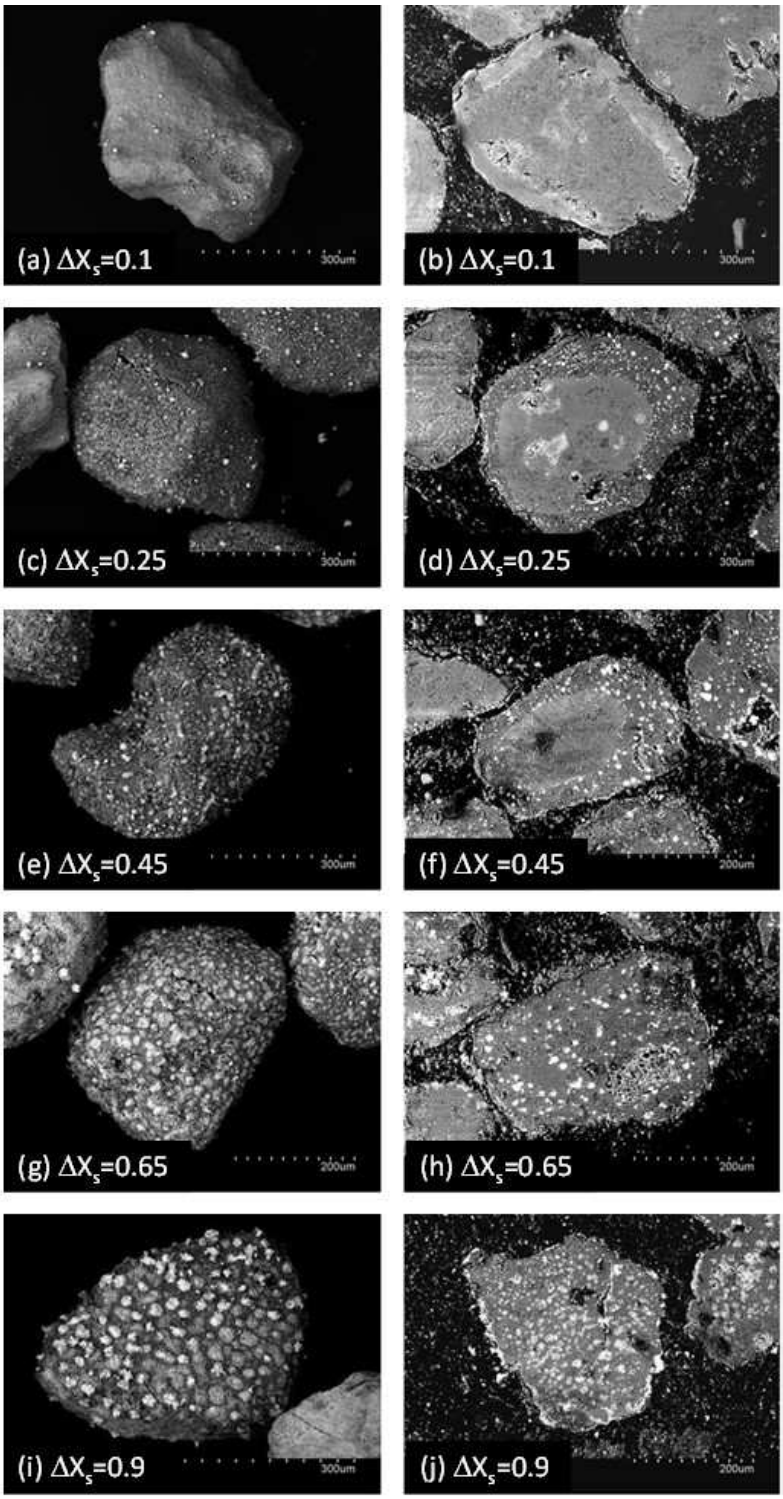

Figure S5. SEM images obtained with backscattered electrons of whole and cross-cut particles as a function of ΔX_s in the redox cycles. Particles highly oxidized in each redox cycle. Reaction temperature: 800 °C.

S.7. SEM images of used particles after redox cycles with the highly oxidized oxygen carrier at 900 °C

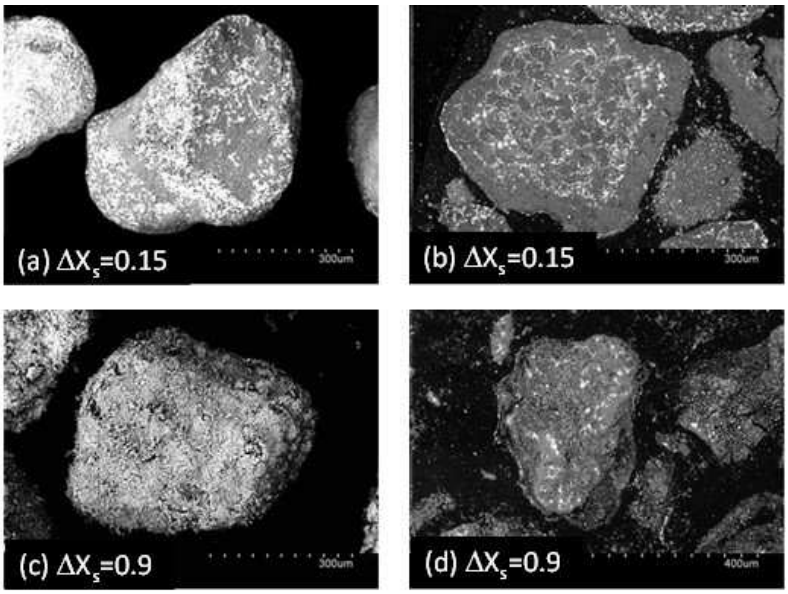

Figure S6. SEM images obtained with backscattered electrons of whole and cross-cut particles as a function of ΔX_s in the redox cycles. Particles highly oxidized in each redox cycle. Reaction temperature: 900 °C.

S.8. Redox cycles with the highly reduced oxygen carrier at 800 °C

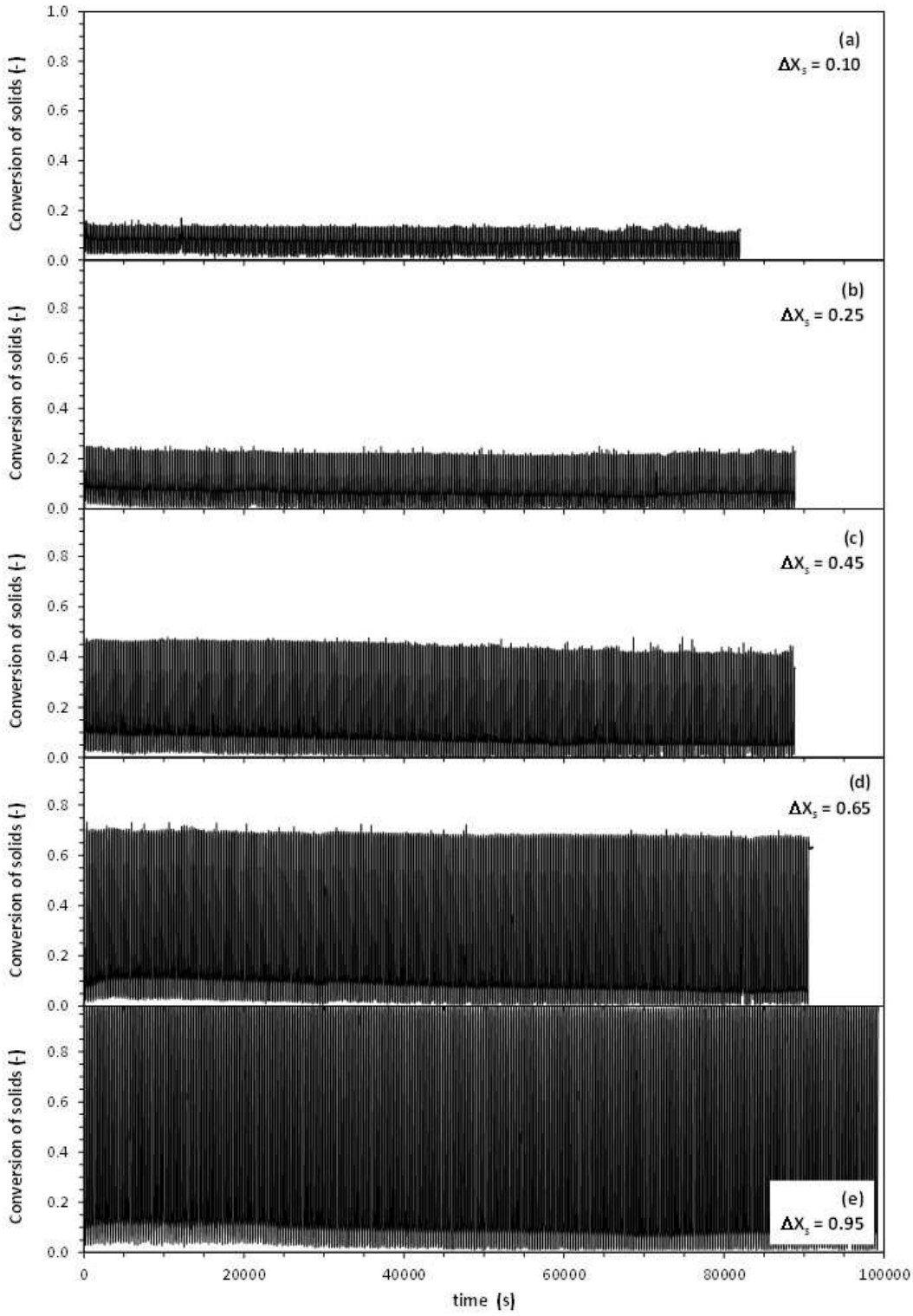

Figure S7. Evolution of solids conversion (defined for oxidation state) during the redox cycles performed at different ΔX_s values with the oxygen carrier being highly reduced in each redox cycle. Reaction temperature: 800 °C.

S.9. Redox cycles with the highly reduced oxygen carrier at 900 °C

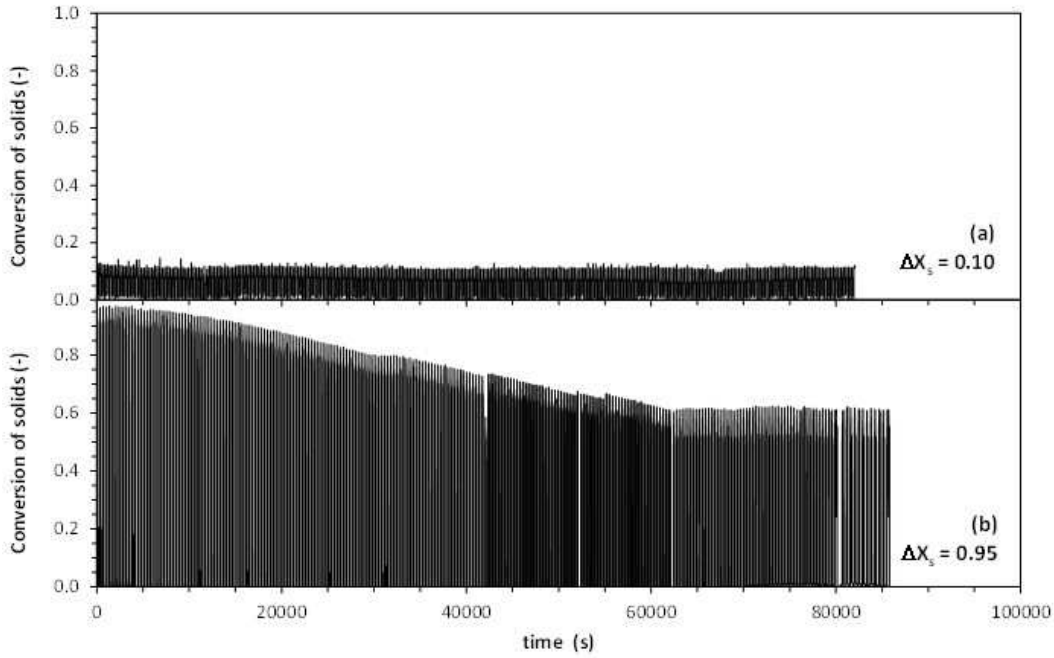

Figure S8. Evolution of solids conversion (defined for oxidation state) during the redox cycles performed at different ΔX_s values with the oxygen carrier being highly reduced in each redox cycle. Reaction temperature: 900 °C.

S.10. XRD patterns corresponding to the highly reduced oxygen carrier at 800 °C

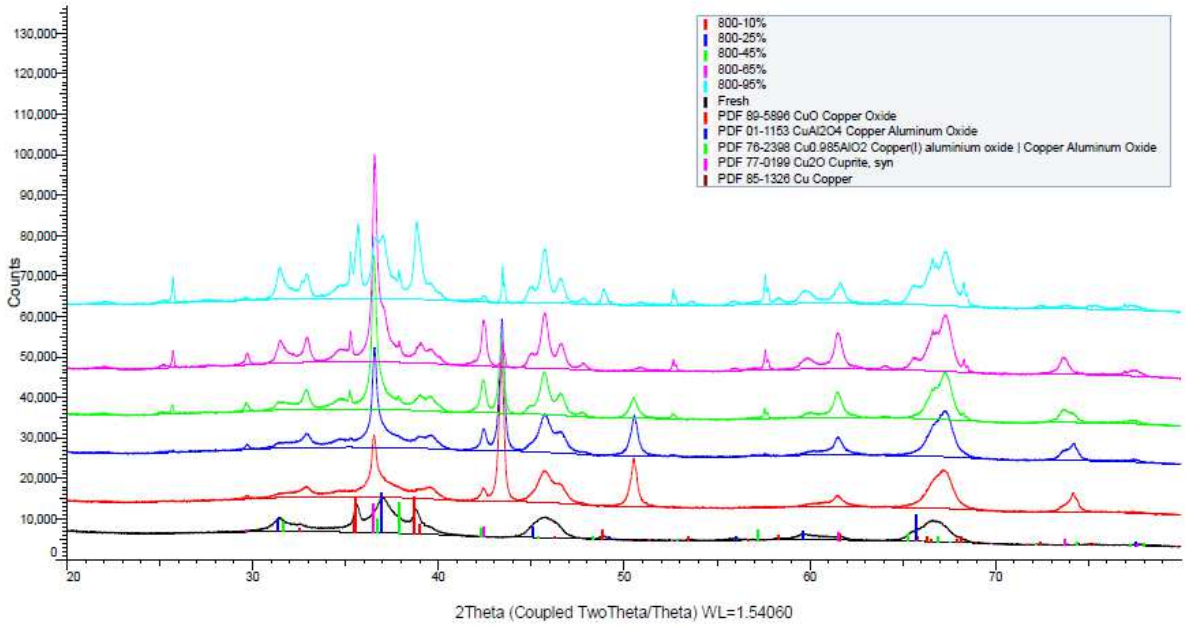

Figure S9. XRD diffractograms of the samples corresponding to the TGA tests performed at 800 ºC with the highly reduced Cu14Al_ICB oxygen carrier (only Cu-compounds are tagged).

S.11. XRD patterns corresponding to the highly reduced oxygen carrier at 900 °C

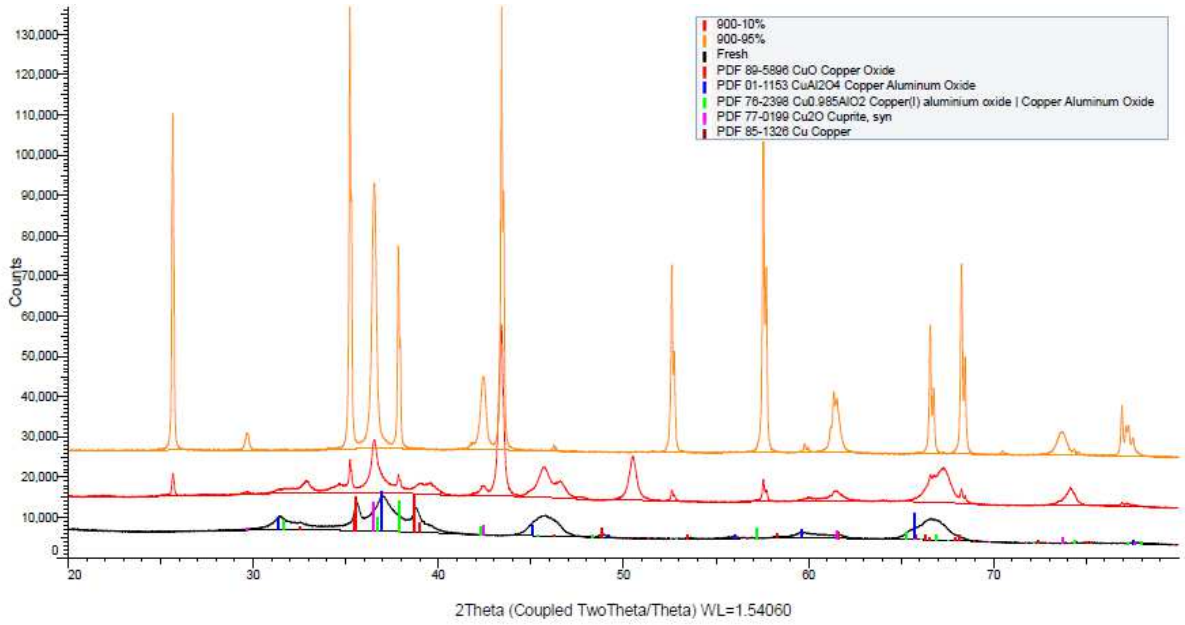

Figure S10. XRD diffractograms of the samples corresponding to the TGA tests performed at 900 ºC with the highly reduced Cu14Al_ICB oxygen carrier (only Cu-compounds are tagged).

S.12. SEM images of used particles after redox cycles with the highly reduced oxygen carrier at 800 °C

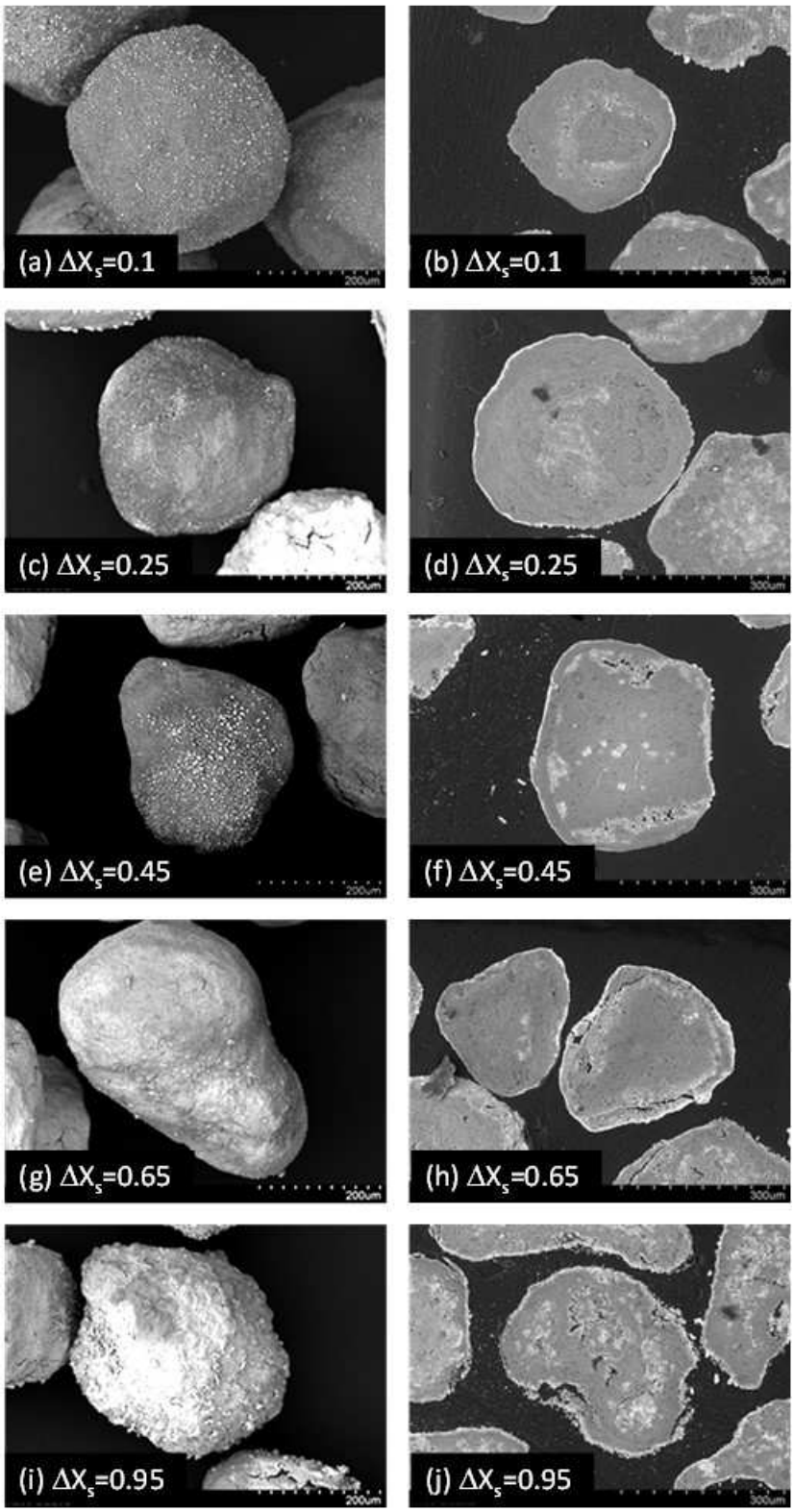

Figure S11. SEM images obtained with backscattered electrons of whole and cross-cut particles as a function of ΔX_s in the redox cycles. Particles fully reduced in each redox cycle. Reaction temperature: 800 °C.

S.13. SEM images of used particles after redox cycles with the highly reduced oxygen carrier at 900 °C.

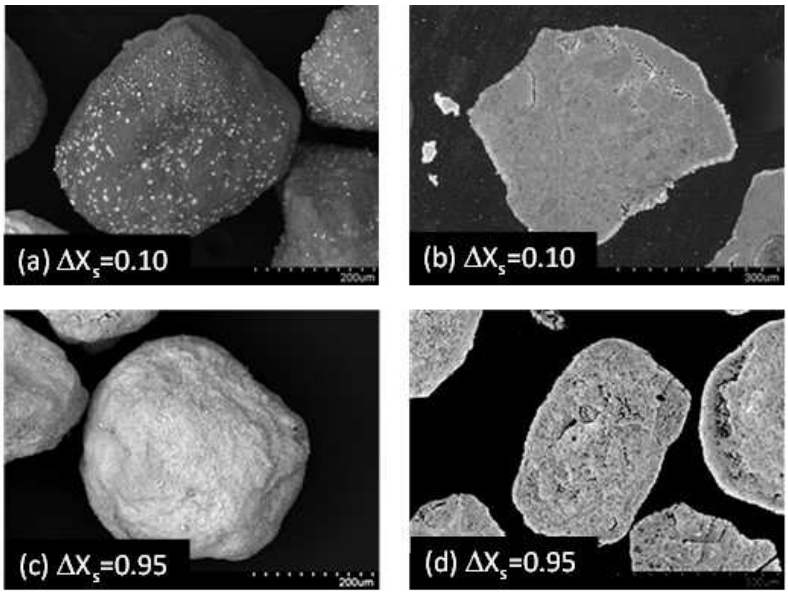

Figure S12. SEM images obtained with backscattered electrons of whole and cross-cut particles as a function of ΔX_s in the redox cycles. Particles fully reduced in each redox cycle. Reaction temperature: 900 °C.

S.14. Ellingham diagram for the Cu14Al_ICB oxygen carrier.

Figure S13 shows the Ellingham diagram corresponding to the reactions involving the Cu14Al_ICB oxygen carrier, summarized in Table 5 of the manuscript. The reduced/oxidized pairs were considered for the oxidation reaction in the Ellingham diagram. In the case that one reaction X in Table 5 involves reduction with H_2, the same reduced/oxidized pair was referred to RX_O2 in the Ellingham diagram.

As a general rule of thumb, in an Ellingham diagram the oxides at the bottom of the diagram can oxidize the oxides at the top and a very negative ΔG value favours direct reactions, whereas a positive (or less negative) ΔG value favours reverse reactions.

Based on the results shown in the diagram, the following considerations regarding the thermodynamics of the system can be drawn:

- All copper oxides and copper aluminates can be reduced by H_2 and, in the presence of this reducing agent, the most stable copper phase is Cu^0, whether the reduction takes place through copper oxides or copper aluminates.
- Copper aluminates are more stable than copper oxides. Specifically, $CuAlO_2$ is more stable than Cu_2O (R9_O2 vs R11), and $CuAl_2O_4$ is more stable than CuO at temperatures above 630 °C (R5_O2 vs R10).
- The reduction to Cu^0 is thermodynamically favoured over the formation of $CuAlO_2$, so the accumulation of the latter in the Cu14Al_ICB oxygen carrier particles when the material is highly oxidized at the beginning of the reduction stage can only be explained by a limitation of reaction kinetics. Therefore, in order to remove the $CuAlO_2$ it is necessary to highly reduce the oxygen carrier particles.
- Regarding the CLOU mechanism, from the Ellingham diagram it is concluded that CLOU reactions are thermodynamically favoured at high temperature both from CuO (R12) and $CuAl_2O_4$ (-R3). Furthermore, the CLOU reaction from $CuAl_2O_4$ is more favoured to $CuAlO_2$ (R3) than to Cu_2O (R16). Besides, CLOU phenomenon through reaction R15 could be more favourable than through

reaction R13. Finally, the CuO + Al_2O_3 system is not stable at temperatures above 1000 ºC, which means that reaction R15 is an alternative path for releasing molecular oxygen in CLC processes that operate with Cu-based oxygen carriers at high temperatures.

- Regarding oxidation reactions, it can be seen that it is easier to oxidize Cu^0 to Cu_2O (R11) than to CuO (R10 and R12), although CuO is stable even at high temperatures.

Finally, it is worth mentioning that R1 and R14 reactions have been included in the Ellingham diagram, although they are not redox reactions, to analyse whether the interaction between copper oxides (CuO and Cu_2O) and alumina is thermodynamically favoured.

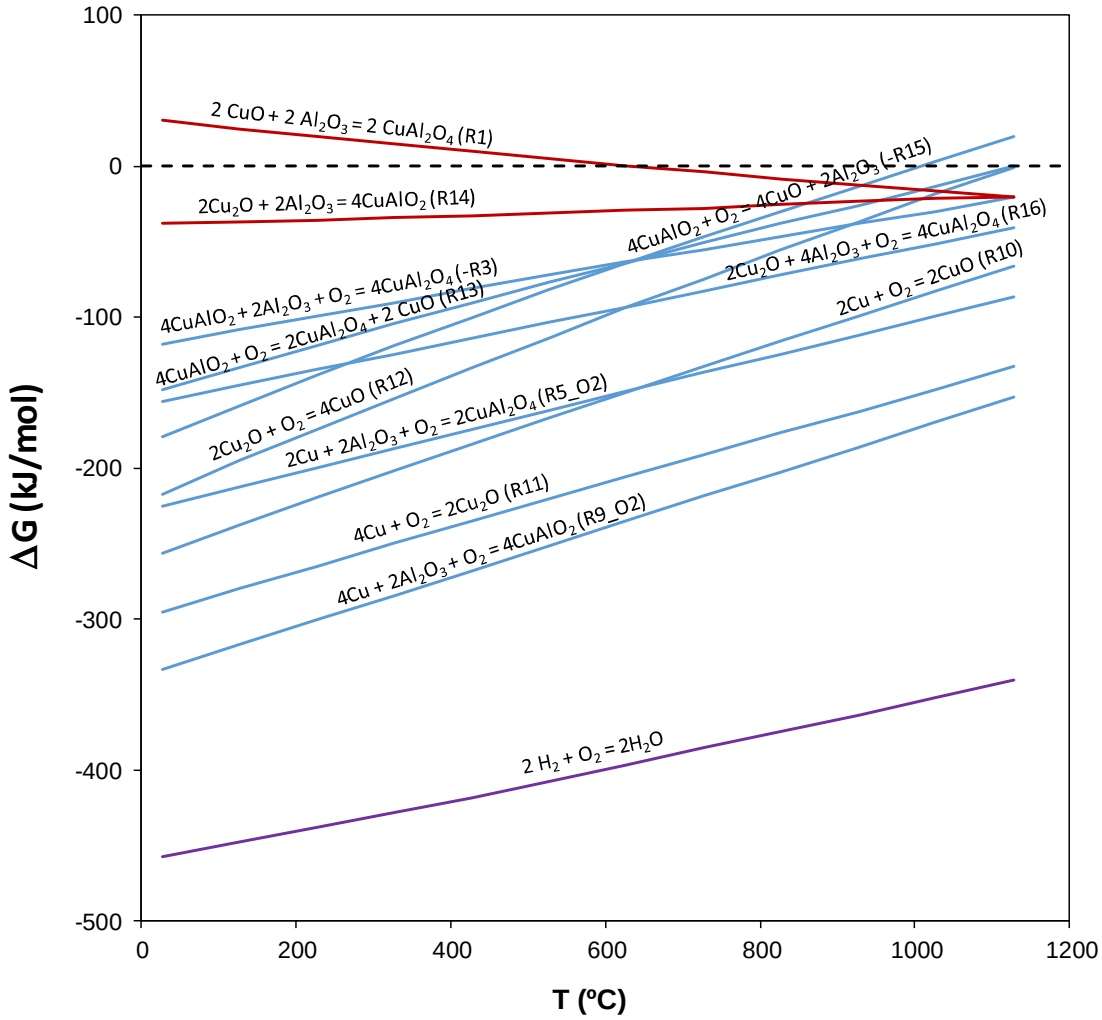

Figure S13. Schematic of the Ellingham diagram for the potential Cu-based species present in the Cu14Al_ICB oxygen carrier. Thermodynamic data were obtained from Barin and Platzki [16] and Jacob and Alcock [17].

S.15. Main physico-chemical characterization results

Table S.2. Summary of the main results achieved during the physico-chemical characterization of aged Cu14Al_ICB material.

HIGHLY OXIDIZED	**800 °C**	**900 °C**
ΔX_s: LOW	✓ Redox stability: GOOD ✓ Reactivity: HIGH ✓ Cu migration: VERY LOW ✓ Crushing Strength: HIGH ✓ δ-Al_2O_3 promoted ✓ $CuAl_2O_4$ promoted (good reducibility) ✓ Amorphous: HIGH	× **Redox stability: POOR** × **Reactivity: LOW (both reduction and oxidation)** ✓ Cu migration: LOW (sintering in the core) ✓ Crushing Strength: HIGH ✓ α-Al_2O_3 promoted × **$CuAlO_2$ promoted (low capability to be oxidized)** ✓ Amorphous: HIGH
ΔX_s: INTERMEDIATE	× **Redox stability: POOR** ✓ Reactivity: HIGH × **Cu migration: YES (increasing with ΔX_s)** ✓ Crushing Strength: HIGH ✓ δ-Al_2O_3 promoted × **$CuAlO_2$ promoted (low capability to be oxidized)** ✓ Amorphous: HIGH	
ΔX_s: HIGH	✓ Redox stability: GOOD ✓ Reactivity: HIGH × **Cu migration: YES (intense)** ✓ Crushing Strength: HIGH ✓ δ-Al_2O_3 promoted ✓ CuO promoted (good reducibility) ✓ Amorphous: HIGH	✓ Redox stability: GOOD ✓ Reactivity: HIGH, **but low at the end of oxidation** × **Cu migration: YES** (but some sintering in the core) × **Crushing Strength: LOW** ✓ α-Al_2O_3 promoted ✓ CuO promoted (good reducibility) × **Amorphous: LOW**
HIGHLY REDUCED	**800 °C**	**900 °C**
ΔX_s: LOW	✓ Redox stability: GOOD ✓ Reactivity: HIGH ✓ Cu migration: VERY LOW ✓ Crushing Strength: HIGH ✓ δ-Al_2O_3 promoted ✓ Cu_2O promoted (good reducibility) ✓ Amorphous: HIGH	✓ Redox stability: GOOD ✓ Reactivity: HIGH ✓ Cu migration: LOW ✓ Crushing Strength: HIGH ✓ δ-Al_2O_3, θ-Al_2O_3 and α-Al_2O_3 promoted ✓ Cu_2O and $CuAl_2O_4$ promoted (good reducibility) ✓ Amorphous: HIGH
ΔX_s: INTERMEDIATE	✓ Redox stability: GOOD ✓ Reactivity: HIGH × **Cu migration: YES (increasing with ΔX_s)** ✓ Crushing Strength: HIGH ✓ δ-Al_2O_3 and θ-Al_2O_3 promoted ✓ Cu_2O and $CuAl_2O_4$ promoted (good reducibility) ✓ Amorphous: HIGH	
ΔX_s: HIGH	✓ Redox stability: GOOD ✓ Reactivity: HIGH × **Cu migration: YES (intense)** ✓ Crushing Strength: HIGH ✓ δ-Al_2O_3, θ-Al_2O_3 and α-Al_2O_3 promoted ✓ Cu_2O, CuO and $CuAl_2O_4$ promoted (good reducibility) ✓ Amorphous: HIGH	× **Redox stability: POOR** ✓ Reactivity: HIGH, **but low at the end of oxidation** × **Cu migration: YES (intense)** × **Crushing Strength: LOW** ✓ α-Al_2O_3 promoted ✓ CuO promoted (then it is reduced to Cu_2O in N_2) × **Amorphous: LOW**

S.16. References

[1] J. Adánez, P. Gayán, J. Celaya, L.F. de Diego, F. García-Labiano, A. Abad, Chemical Looping Combustion in a 10 kW_{th} Prototype Using a CuO/Al_2O_3 Oxygen Carrier: Effect of Operating Conditions on Methane Combustion, Ind. Eng. Chem. Res. 45 (2006) 6075-6080.

[2] L.F. de Diego, F. García-Labiano, P. Gayán, J. Celaya, J.M. Palacios, J. Adánez, Operation of a 10 kW_{th} chemical-looping combustor during 200 h with a $CuO–Al_2O_3$ oxygen carrier, Fuel 86 (2007) 1036–1045.

[3] F. García-Labiano, P. Gayán, J. Adánez, L.F. de Diego, C.R. Forero, Solid Waste Management of a Chemical-Looping Combustion Plant using Cu-Based Oxygen Carriers, Environ. Sci. Technol. 41 (2007) 5882-5887.

[4] M.T. Izquierdo, F. García-Labiano, A. Abad, A. Cabello, P. Gayán, L.F. de Diego, J. Adánez, On the optimization of physical and chemical stability of a Cu/Al_2O_3 impregnated oxygen carrier for chemical looping combustion, Fuel Processing Technology 215 (2021) 106740.

[5] L.F. de Diego, F. García-Labiano, P. Gayán, A. Abad, A. Cabello, J. Adánez, G. Sprachmann, Performance of Cu- and Fe-based oxygen carriers in a 500 W_{th} CLC unit for sour gas combustion with high H_2S content, International Journal of Greenhouse Gas Control 28 (2014) 168-179.

[6] C.R. Forero, P. Gayán, F. García-Labiano, L.F. de Diego, A. Abad, J. Adánez, High temperature behaviour of a $CuO/\gamma Al_2O_3$ oxygen carrier for chemical-looping combustión, Int. J. Greenhouse Gas Control 5 (2011) 659–667.

[7] C.R. Forero, P. Gayán, F. García-Labiano, L.F. de Diego, A. Abad, J. Adánez, Effect of gas composition in Chemical-Looping Combustion with copper-based oxygen carriers: Fate of sulphur, Int. J. Greenhouse Gas Control 4 (2010) 762-770.

[8] C.R. Forero, P. Gayán, L.F. de Diego, A. Abad, F. García-Labiano, J. Adánez, Syngas combustion in a 500 W_{th} Chemical-Looping Combustion system using an impregnated Cu-based oxygen carrier, Fuel Process. Technol. 90 (2009) 1471–1479.

[9] P. Gayán, C.R. Forero, L.F. de Diego, A. Abad, F. García-Labiano, J. Adánez, Effect of gas composition in Chemical-Looping Combustion with copper-based oxygen carriers: Fate of light hydrocarbons, Int. J. Greenhouse Gas Control 4 (2010) 13-22.

[10] S. Penthor, F. Zerobin, K. Mayer, T. Pröll, H. Hofbauer, Investigation of the performance of a copper based oxygen carrier for chemical looping combustion in a 120 kW pilot plant for gaseous fuels, Appl. Energy 145 (2015) 52–59.

[11] J. Haus, E.-U. Hartge, J. Werther, S. Heinrich, Effects of a Two-Stage Fuel Reactor on Chemical Looping Combustion with Methane, Bituminous Coal, Lignite and Wood Biomass, Proc. 5th Int. Conf. Chemical Looping, 2018, Park City, Utah, USA.

[12] A. Cabello, P. Gayán, A. Abad, L.F. de Diego, F. García-Labiano, M.T. Izquierdo, A. Scullard, G. Williams, J. Adánez, Long-lasting Cu-based oxygen carrier material for industrial scale in Chemical Looping Combustion, Int. J. Greenhouse Gas Control 52 (2016) 120–129.

[13] R.F. Pachler, K. Mayer, S. Penthor, M. Kollerits, H. Hofbauer, Fate of sulfur in chemical looping combustion of gaseous fuels using a copper-based oxygen carrier, Int. J. Greenhouse Gas Control 71 (2018) 86–94.

[14] Ø. Langørgen, I. Saanum, N.E.L. Haugen, Chemical looping combustion of methane using a copper-based oxygen carrier in a 150 kW reactor system, Energy Procedia 114 (2017) 352–360.

[15] A. Lambert, A. Tilland, W. Pelletant, S. Bertholin, F. Moreau, I. Clemençon, M. Yazdanpanah, Performance and degradation mechanisms of CLC particles produced by industrial methods, Fuel 216 (2018) 71–82.

[16] I. Barin, G. Platzki, Thermochemical Data of Pure Substances, VCH, Weinheim, Germany (1995).

[17] K.T. Jacob, C.B. Alcock, Thermodynamics of $CuAlO_2$ and $CuAl_2O_4$ and phase equilibria in the system Cu_2O–CuO–Al_2O_3. J. Am. Ceram. Soc. 58 (1975) 192-195.